Adsorption and Interfacial Chemistry of Pentacene on the Clean Si(100) Surface: A Density Functional Study

Francesca Nunzi,*,† Antonio Sgamellotti,† Cecilia Coletti,‡ and Nazzareno Re*,‡

Istituto di Scienze e Tecnologie Molecolari (ISTM-CNR), c/o Dipartimento di Chimica, Università di Perugia, I-06123 Perugia, Italy, and Dipartimento di Scienze del Farmaco, Università G. d'Annunzio, I-66100 Chieti, Italy

Received: October 10, 2007; In Final Form: January 18, 2008

Density functional theory calculations have been performed on the main adsorption configurations of pentacene on the Si(100) surface and on the possible pathways for the following C−H bond cleavage. We considered possible candidates for all the orientations of pentacene experimentally observed with STM, i.e., on the top of silicon dimer rows, perpendicular to the dimer rows, diagonal to the dimer rows and between two adjacent dimer rows ("in between"). Our calculations indicate that the most stable adsorption configuration of pentacene on the Si(100) surface is the symmetric perpendicular structure with an adsorption energy of −128.3 kcal mol^{-1}, with the in between structure 10.5 kcal mol^{-1} and the symmetric parallel structure 13.0 kcal mol^{-1} higher in energy. Transition states for the dissociation of C−H and formation of Si−H bonds from the main adsorption configurations of pentacene have been characterized and the corresponding energy barriers estimated. We identified two kinds of adsorbed configurations of pentacene from which the breaking of two C−H bonds can be accessible: one on top of a silicon dimer row with one or both outer benzene rings di-σ−bonded through a [2 + 2] cycloaddition; one with one or more pentacene rings 1,4 di-σ-bonded across two dimer rows, such as the in between structure. The kinetically most favorable reactive channel is that from the in between configuration and involves the separate abstraction of two hydrogen atoms on the sp^3 carbon atoms by the two silicon atoms of the two dimers bearing an unpaired electron, with an energy barrier of 29−30 kcal mol^{-1}.

Introduction

Organic monolayers and thin films on surfaces have been attracting much interest in the effort to develop new electronics by applying the functionality of organic materials to the well-established silicon-based devices and expand conventional microelectronics technology.[1,2] In particular, thin films of semiconducting organic molecules have been considered the starting point to develop electronic devices such as organic thin-film transistors.[3−5]

The Si(100) surface constitutes the most important substrate for fabrication of the integrated circuits used in microprocessors and memory chips.[6,7] Due to its special structural and electronic properties,[8,9] such as the close analogy of Si dimers to a C−C double bond, this surface provides an ideal platform for building hybrid devices through the attachment of unsaturated hydrocarbons on the template generated by the peculiar pattern of Si dimer rows on the Si(100) 2 × 1 reconstructed surface.[10]

Among the possible organic semiconducting candidates, one of the most promising is pentacene ($C_{22}H_{14}$), a planar molecule composed of five fused aromatic rings. Indeed, its planarity allows the formation of highly ordered crystal structures[11−13] with high field-effect mobility.[14,15] For these reasons, a considerable amount of work has recently been carried out on the growth of pentacene thin films to investigate the changes in chemical and electronic structure that occur when pentacene is deposited onto clean and chemically modified Si(100) surfaces.[16−26]

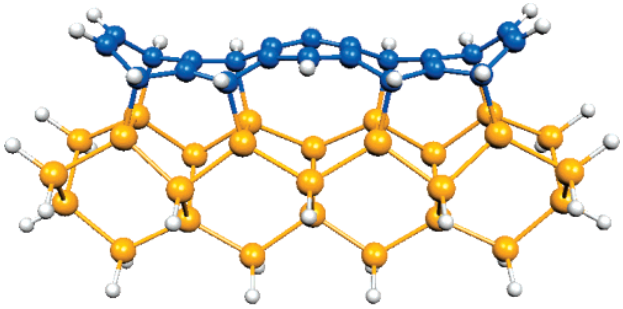

19

Figure 1. Optimized geometry for the pentacene molecule adsorbed on top of the rows of the Si(100) surface through two [4 + 2] and two [2 + 2] additions.

Highly crystalline thin films with large grain sizes were recently prepared through the layer-by-layer growth of pentacene on both clean and organically modified Si(100) surfaces.[3,16] Several studies showed that when pentacene is deposited directly on the Si(100) surface, the first molecular layer strongly interacts with the surface dangling bonds and that subsequent two-dimensional film growth occurs through molecular deposition on the top of this initial chemisorbed layer.[19−21] The formation of such chemisorbed layer inhibits the nucleation of pentacene crystals on clean Si(100) surface, and indeed, the passivation of the reactive silicon surface with cyclopentene prior to pentacene deposition has been observed to improve nucleation and growth of crystalline thin films with better electronic

* To whom correspondence should be addressed. E-mail: nunzi@thch.unipg.it (F.N.); nre@unich.it (N.R.). Fax: +39 0755855606 (F.N.); +39 08713554614 (N.R.).
† Università di Perugia.
‡ Università G. d'Annunzio.

10.1021/jp709892q CCC: $40.75
Published on Web 03/21/2008

SCHEME 1: Bonding Configurations for the Adsorption of Pentacene on One Dimer of the Si(100) Surface

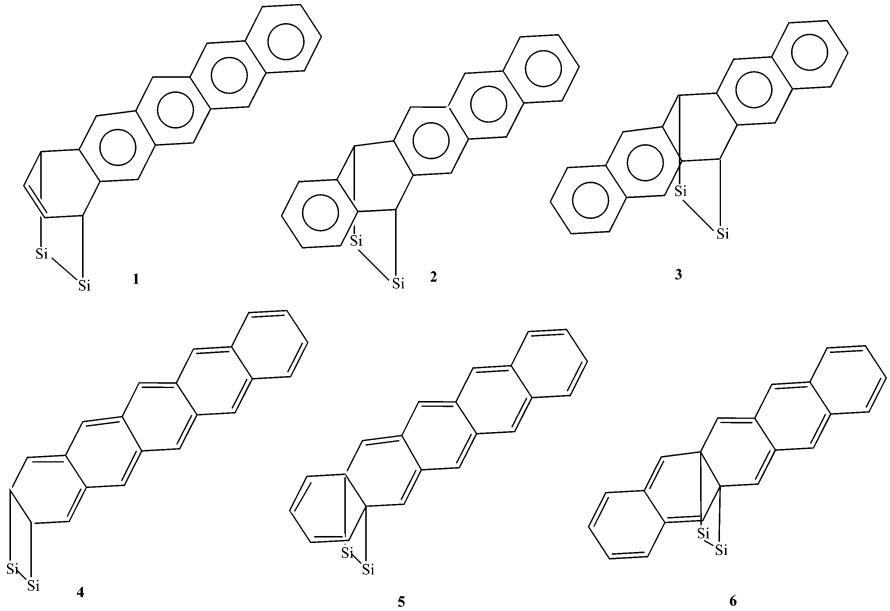

SCHEME 2: Bonding Configurations for the Adsorption of Pentacene on Two Dimers on the Same Row of the Si(100) Surface

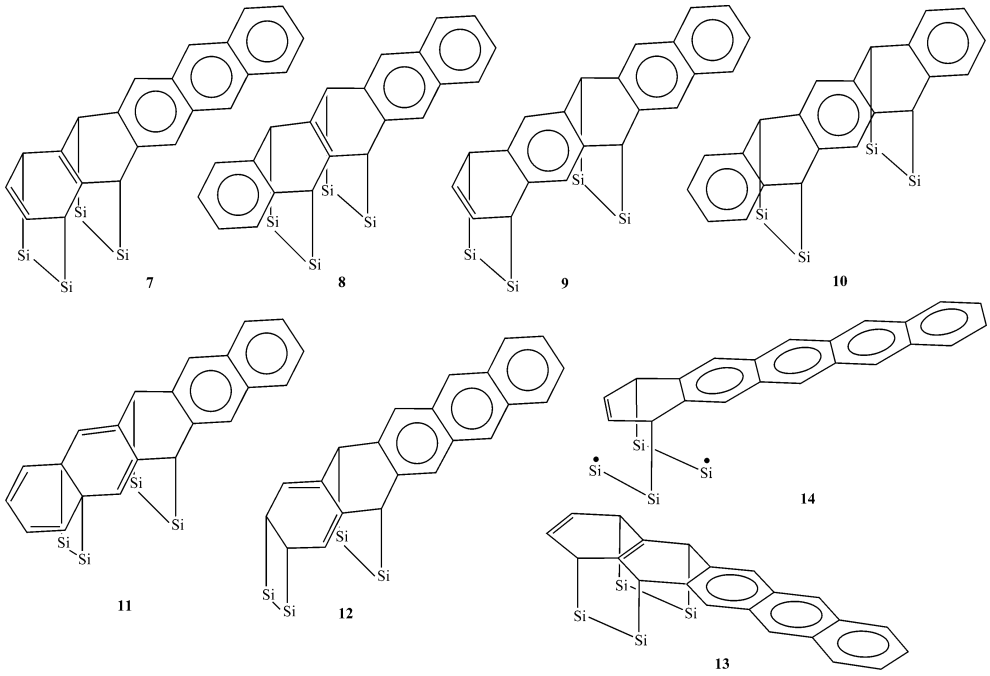

properties. An understanding of the interaction between pentacene molecules and the silicon Si(100) surfaces is therefore of fundamental importance for the control of the pentacene growth.

The adsorption of pentacene on the Si(100) surface has been studied by several techniques, such as scanning tunneling microscopy (STM), Fourier transform infrared spectroscopy (FTIR), ultraviolet photoelectron spectroscopy (UPS), and core-level photoemission spectroscopy.[19−22] These studies have confirmed that the first adsorbed layer of pentacene molecules involves the formation of strong Si−C bonds, while the subsequent layers consist of pentacene molecules only weakly bound to the surface. Low-coverage STM has provided a range of possible orientations with respect to the underlying dimer rows in which the pentacene molecules could adsorb flat onto the silicon surface. In particular, the submonolayer STM study of Kasaya et al.[19] has shown three distinct orientations for pentacene adsorbed onto the silicon surface, with the molecules lying parallel to the silicon dimer rows (type A), perpendicular to the dimer rows (type B), and diagonal to the dimer rows (type C). The populations of the oriented molecules were estimated nearly similar for types A and B, respectively 27% and 35%, and much lower for type C, ca. 5%, while the residual population could not be categorized. A careful magnification of these images allowed one to distinguish characteristic differences within both types A and B adsorption orientations. For type A orientation the high-resolution images showed an A-1 subtype, where the molecular image is divided into two

CHART 1

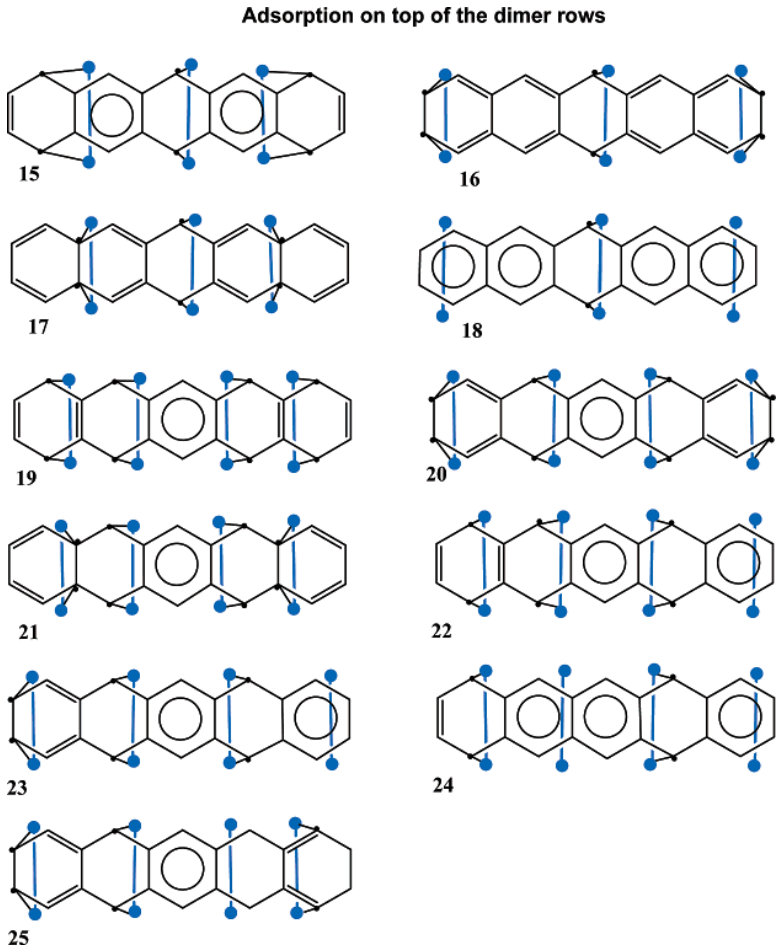

TABLE 1: Binding Energies (in kcal mol^{-1}) for the Main Adsorption Configurations of Pentacene on One and Two Adjacent Silicon Dimers on the Same Row of the Si(100) Surface[a]

one dimer						two dimers							
1	**2**	**3**	**4**	**5**	**6**	**7**	**8**	**9**	**10**	**11**	**12**	**13**	**14**
−40.3	−56.3	−60.1	20.3	37.3	42.4	−72.0	−86.2	−71.2	−81.9	−24.4	−48.4	−69.1	−19.2

[a] See Schemes 1 and 2.

TABLE 2: Binding Energies (in kcal mol^{-1}) for the Main Adsorption and C−H Broken Configurations of Pentacene on the Si(100) Surface[a]

On top										
15	**16**	**17**	**18**	**19**	**20**	**21**	**22**	**23**	**24**	**25**
−80.4	50.9	13.9	−60.9	−115.3	−67.0	−21.0	−99.4	−74.0	−81.1	−72.8

Perpendicular								Diagonal		In-between
26	**27**	**28**	**29**	**30**	**31**	**32**	**33**	**40**	**43**	**44**
−128.3	−21.0	−62.9	−95.6	−98.6	−84.6	−30.4	−5.6	−79.7	−35.9	−117.8

On top	C−H broken				
45	**46**	**47**	**48**	**49**	**50**
−71.1	−92.8	−114.3	−160.8	−141.6	−140.3

[a] See Charts 1−3 and Figures 1−4.

parts at the center, and an A-2 subtype, where the molecular image is divided into three nearly equal parts. Moreover, in the same high-resolution image, A-1 and A-2 subtypes were seen to exist concurrently with an unresolved type A image, making it unclear whether these subtypes were the result of a resolution issue or represented different structures. For type B orientation the high-resolution images also showed a B-1 subtype, where the molecular image is divided symmetrically into two parts at the center, and a B-2 subtype, where the molecular image is divided into three unequal parts. More recent STM studies have

CHART 2

Adsorption perpendicular to the dimer rows

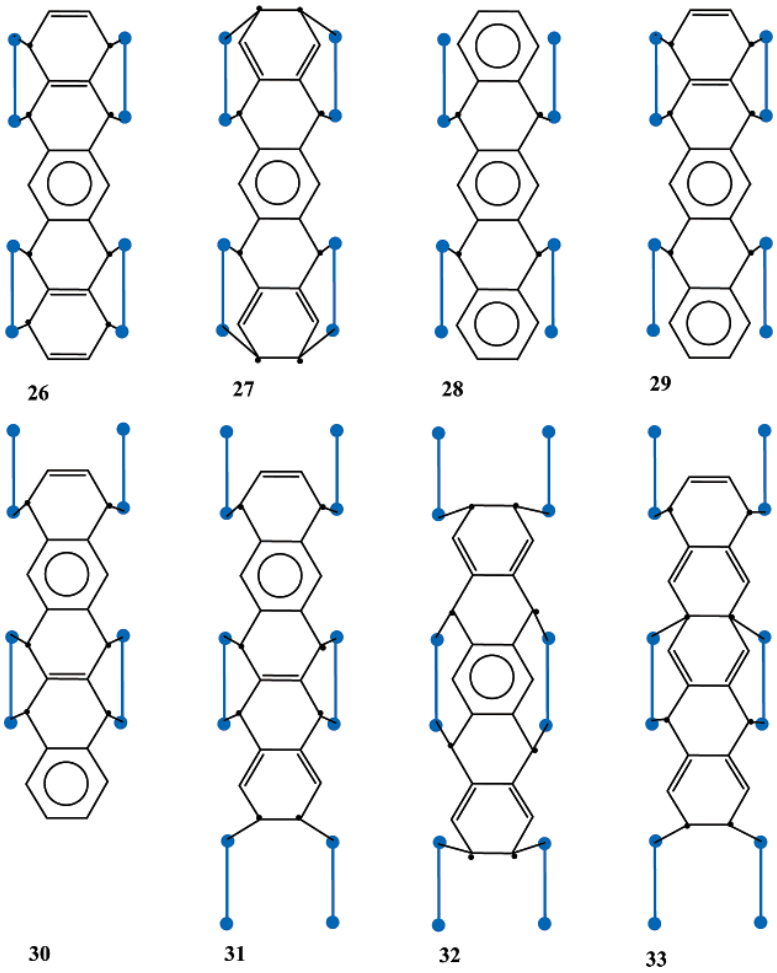

found similar results, although with some minor differences. The study of Suzuki et al.[20] showed evidence for the same A-1, A-2, B-1, and B-2 subtypes and C types in similar ratio (except A-2, which occurs with a very low ratio), while a new A subtype site, called A-3, and a new adsorption site, ''in between'' the dimer rows, were also reported. The study by Hughes et al.[21] also found evidence for the same type A and B configurations, although the issue of subtypes was not resolved. However, in contrast to the studies of Kasaya et al. and Suzuki et al., no adsorption site diagonal to the dimer rows, type C, could be observed, while the adsorption sites in between the dimer rows were reported. The populations of type A and B adsorption sites were found to be nearly equal, with in between dimer sites accounting for half this number.

Moreover, recent FTIR and UPS studies have shown that the initial layer of pentacene involves a certain amount of dissociation of the adsorbed molecules.[22] Indeed, FTIR spectroscopy has shown the presence of Si−H vibrational modes at 2091 cm^{-1}, which indicate that some of the pentacene C−H bonds are cleaved upon adsorption with consequent hydrogenation of some of the surface silicon atoms. This cleavage leads to the irreversible adsorption of pentacene molecules to the Si(100) surface, and indeed, the initial interfacial layer is stable upon heating up to 400 K, showing fragmentation rather than desorption at higher temperatures. These results contrast with those reported for benzene, which can be reversibly adsorbed onto and desorbed from Si(100) surface without any evidence of C−H dissociation.[27,28]

In spite of the intense experimental activity, the nature of the interaction of pentacene onto the clean Si(100) surface, the detailed geometry of its adsorption configurations, and the features of the dissociation processes possibly occurring upon adsorption are not yet fully understood and accurate theoretical investigation could provide invaluable insights into the chemisorption of pentacene on this silicon surface.

A few theoretical works have recently been performed on the adsorption of pentacene on silicon surface,[22−25] but all have been carried out at essentially semiempirical level, except ref 20. Furthermore, none of them addressed the issue of the pentacene dissociation on the silicon surface.

In this work, we report an extensive density functional theory (DFT) investigation of the main adsorption configurations of pentacene on the Si(100) surface and of the possible pathways for the following C−H bond cleavage. Several adsorption sites of the possible A−C and in between the rows types have been considered and fully optimized, allowing an evaluation of their relative thermodynamical stabilities. Transition states for the formation of Si−H bonds from the main adsorption configurations of pentacene have been characterized and the corresponding energy barriers estimated. This search has been guided by the results of a recent investigation of the authors on the dissociative adsorption of benzene on the Si(100) surface

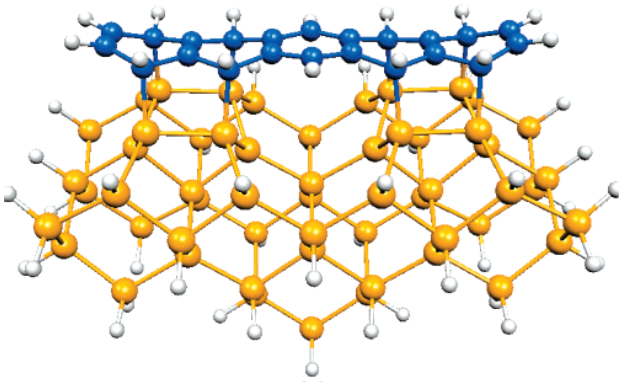

26

Figure 2. Optimized structure for the pentacene molecule adsorbed perpendicular to the dimer rows of the Si(100) surface through four [4 + 2] additions.

showing that C−H cleavage is feasible only from the in between and, although with a higher barrier, from the 1,2 adsorption modes.[29]

Computational Details

The Si(100) surface has been modeled by finite cluster models of various size, ranging from two up to eight silicon dimers, arranged on one, two, or three adjacent rows of the reconstructed 2 × 1 silicon surface and including down to six layers. The top layer consists of pair of silicon atoms, representing the surface dimers, while the remaining subsurface silicon atoms are saturated by hydrogen atoms to avoid dangling bond effects. Although the terminating hydrogen atoms may create a chemical environment different from that of the actual Si(100)-2 × 1 surface at the cluster boundary, a study on cluster models of various sizes has shown that the error is insignificant.[30]

All the adsorption structures have been optimized without any geometrical constraints, and frequency calculations have been performed to check the nature of the stationary points (minima or transition states).

All the electronic structure calculations in this work have been performed with the Jaguar[31] program package, employing the B3LYP exchange-correlation functional[32−34] for the exchange and correlation energies. Unrestricted (UB3LYP) calculations have been performed for the structures with one or more radical character. The B3LYP functional has been used extensively in the past few years to calculate binding and activation energies of organic reactions on Si(100) surfaces using the cluster approximation.[29,35−39] The performance of this functional in predicting the reaction barriers and energies has been assessed against large thermochemistry and themochemical kinetics experimental databases.[40,41] These benchmarks indicate that B3LYP reproduces pretty well reaction enthalpies and atomization energies with mean errors of 1−5 kcal mol^{-1} while systematically underestimating energy barriers by 2−6 kcal mol^{-1}, depending on the basis set and the considered database. Moreover, within the considered databases, B3LYP has given more reliable results for pericyclic reactions of hydrocarbons[40] and for hydrogen transfer reactions,[41] the kinds of reactions occurring on the Si(100) surface that we considered in our work. Although these mean errors are larger than the "chemical accuracy" of 1−2 kcal mol^{-1}, they are small enough to make B3LYP reliable in reproducing, though not always quantitatively experimental, data. Jaguar is computationally very efficient employing all electron basis sets, so that a 6-31G(d,p) basis set was employed for all atoms.

The adsorption energies are calculated as the difference between products and reactants energies in their optimized ground state.

Results and Discussion

Several potential configurations for the adsorption of pentacene on the Si(100) surface, suggested in previous experimental and theoretical studies, were examined. We considered possible candidates for all the orientations of pentacene experimentally observed with STM, i.e., type A (on the top of silicon dimer rows), type B (perpendicular to the dimer rows), type C (diagonal to the dimer rows), and "in between" (between two adjacent dimer rows). In this study we considered 11 configurations of type A, 8 of type B, 10 of type C, and 1 in between, plus many adsorption configurations on a two-dimer cluster model and several further C−H cleaved structures.

A. Adsorption of Pentacene on One and Two Dimers. As preliminary test, we performed DFT calculations on the main adsorption configurations of pentacene on one and two adjacent silicon dimers on the same row of Si(100) (see Schemes 1 and 2, respectively), employing the small two-dimer $Si_{15}H_{16}$ as model cluster, in order to analyze and possibly disentangle the bond energy and steric factors affecting the strength of the adsorption at the interface. The computed adsorption energies are reported in Table 1.

We first considered all the possible adsorption configurations of pentacene involving only one cycloaddition on one silicon dimer with the formation of two Si−C bonds on one benzene rings of the acene molecule (see Scheme 1). Two kinds of σ-bonded adsorption configurations are possible corresponding to a [2 + 2] or a [4 + 2] Diels−Alder-like cycloaddition of a benzene ring with a Si═Si surface dimer. Our results show that the [4 + 2] cycloadditions, **1**−**3**, are thermodynamically favored by 40−60 kcal mol^{-1}, while the [2 + 2] cycloadditions, **4**−**6**, are unfavorable by 20−40 kcal mol^{-1}, as it expected on the basis of the previous study on the adsorption of benzene on the Si(100) surface.[42] The instability of the latter group of adsorption configurations is probably due to the impossibility for any of the six-membered rings to reach the aromaticity. Three different [4 + 2] cycloadditions are possible, on the first (**1**), second (**2**), or third central ring (**3**), the latter being slightly more favorable by 5−20 kcal mol^{-1}. There are also three distinct [2 + 2] cycloadditions, again on the first (**4**), second (**5**), or third ring (**6**), but in this case the addition on the outer ring is less unfavorable by 5−20 kcal mol^{-1}.

We then considered the adsorption of pentacene involving one/two cycloadditions on two silicon dimers, selecting the most significant adsorption configurations with at most one unfavorable [2 + 2] cycloaddition; see Scheme 2. In particular, structures **7**−**10** show two [4 + 2] cycloadditions, while **11** and **12** show [2 + 2] and [4 + 2] cycloadditions. The former group is by far thermodynamically more stable than the latter by 20−60 kcal mol^{-1}.

Two further conclusions can be drawn by comparing the thermodynamic stability of structures **7**−**10**. For instance, the different stability of **7** (−72.0 kcal mol^{-1}) with respect to **8** (−86.2 kcal mol^{-1}) and of **9** (−71.2 kcal mol^{-1}) with respect to **10** (−81.9 kcal mol^{-1}) gives us useful information on the effect of the aromaticity on the adsorption of acenes on the Si(100) surface. Indeed, since it is well-known from previous studies[43] on aromatic compounds that the aromatic stabilization energy of *n*-fused benzene rings is lower than the aromatic stabilization energy of *n* isolated benzene molecules, it can be foreseen that the thermodynamically most stable adsorption

CHART 3

Adsorption diagonal to the dimer rows

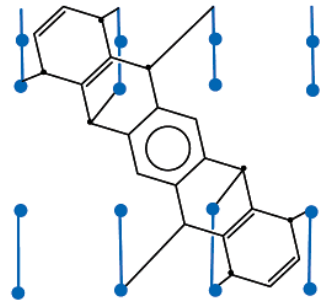
34

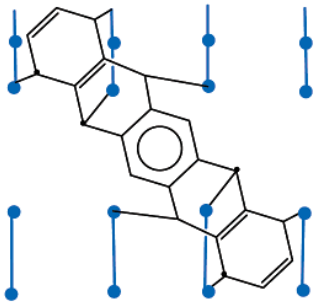
35

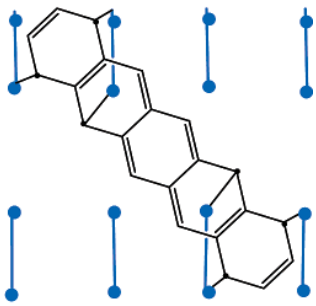
36

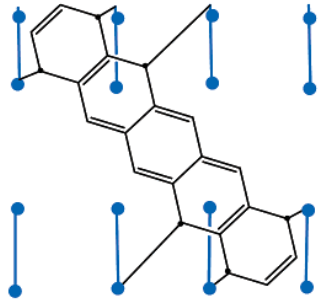
37

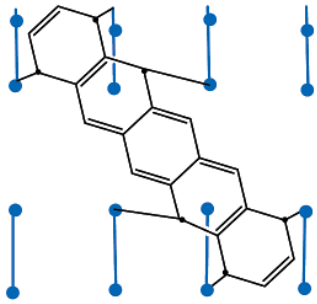
38

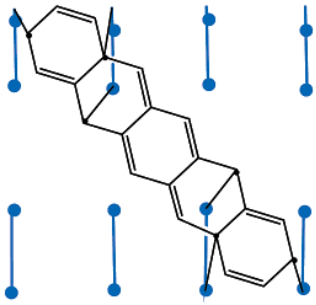
39

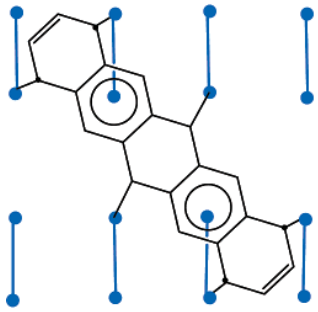
40

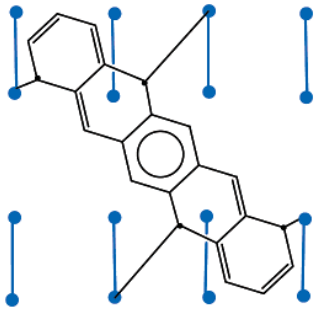
41

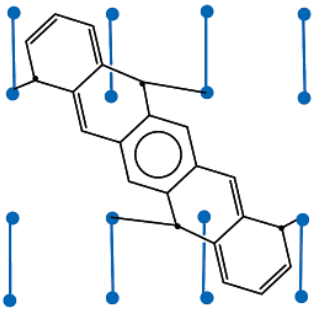
42

Adsorption in-between two dimer rows

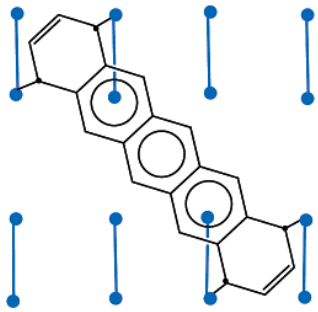
43

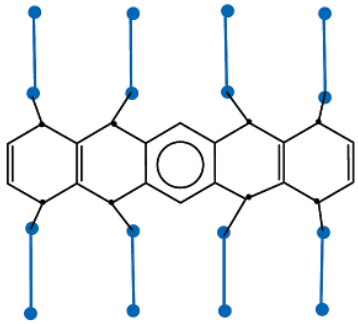
44

configurations of pentacene are those with the highest number of isolated benzene rings. According to this rationale, structure **8**, where one and two-fused benzene rings are maintained after the Si−C bonds formation, is 14.2 kcal mol^{-1} more stable than **7**, where three-fused benzene rings are present. Analogously, **10**, with three isolated benzene rings, is 10.7 kcal mol^{-1} more stable than **9**, showing one- and two-fused benzene rings. In second place, by comparison of the binding energies of **8** (−86.2 kcal mol^{-1}) and **9** (−71.2 kcal mol^{-1}), a gain in energy of 15.0 kcal mol^{-1} is observed for **8**, so that we can state that, for the same aromaticity pattern, the adsorption of pentacene on the Si(100) surface is energetically favored on two adjacent benzene rings, since it allows a minor distortion of the underlying dimers array. Indeed, the Si−Si interdimer distance of 4.038 Å fits

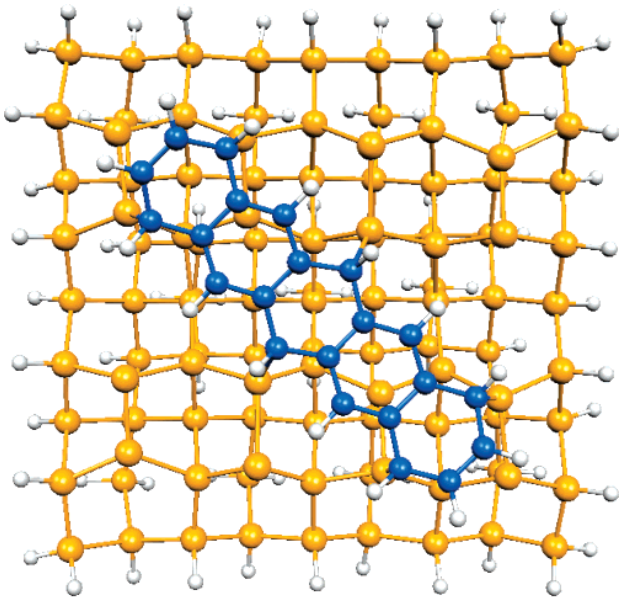

40

Figure 3. Optimized structure for the pentacene molecule adsorbed diagonal to the dimer rows of the Si(100) surface.

better the bonding geometry around the sp^3 carbon atoms on two adjacent rings in **8** than on two rings with one ring in between in **9**.

For the adsorption configurations involving one [2 + 2] cycloaddition, **11** and **12**, a higher thermodynamical stability is associated with the presence of a higher number of aromatic rings as shown by the higher thermodynamic stability of **12** (three aromatic rings, −48.4 kcal mol^{-1}) with respect to **11** (two aromatic rings, −24.4 kcal mol^{-1}). We also considered structure **13**, involving two [4 + 2] cycloadditions but with the pentacene moiety lying perpendicularly to the dimers row, see Scheme 2, which is only 2.9 kcal mol^{-1} higher in energy than **7**, showing essentially the same strain energy contribution. Finally we considered structure **14** in which a benzene ring undergoes a [4 + 2] cycloaddition diagonally across two silicon dimers, leaving two unpaired electrons on the two dangling surface silicon atoms; see Scheme 2. This structure shows an adsorption energy of −19.2 kcal mol^{-1}, higher than that (−40.3 kcal mol^{-1}) for the adsorption of the same terminal ring on a single dimer **1**, probably due to the diradical nature and/or a higher strain energy.

B. Adsorption of Pentacene on Extended Cluster Models. *Adsorption on the Top of a Dimer Row.* On the basis of the observed STM images,[19] we considered 11 bonding configurations for the adsorption of pentacene on the top of a dimer row, type A; see Chart 1 and Table 2 for the computed adsorption energies. Structures **15**−**18** involve the pentacene molecule adsorbed with its center located on the top of a dimer and interacting with up to three underlying dimers and are therefore good candidates for subtype A-1 images, split into two parts. On the other hand, in **19**−**25** pentacene is adsorbed with its center located between two dimers and interacting with up to four underlying dimers so that these structures are good candidates for subtype A-2 images, split into three sections.

In structures **15**−**17**, pentacene is attached through three pairs of Si−C bonds between the three surface silicon dimers of the $Si_{18}H_{22}$ cluster and the central and the two outer rings of pentacene. The central ring is bound through a [4 + 2] cycloaddition, while the outer rings are bound through [4 + 2] cycloadditions in **15** and through [2 + 2] cycloadditions in **16** and **17**. On the other hand, in **18** only the central ring is bound through a [4 + 2] cycloaddition. Due to these different bonding schemes, two isolated aromatic rings are left in **15** and none in **16** and **17**, which are therefore expected to be less stable. Indeed, as it is shown in Table 2, adsorption energies of −80.4, +50.9, and +13.9 kcal mol^{-1} have been calculated for **15**−**17**, respectively, showing that structure **15**, involving only [4 + 2] cycloadditions, is 90−130 kcal mol^{-1} more stable in energy than **16** and **17**. On the other hand, two two-fused rings are left in **18**, which accordingly is only 19.5 kcal mol^{-1} higher than **15**.

In **19**−**21**, pentacene is attached through four pairs of Si−C bonds between the four surface silicon dimers of the $Si_{23}H_{26}$ model and four of the five pentacene rings, leaving the central ring aromatic. The two innermost rings are bound through a [4 + 2] cycloaddition, while the outermost rings are bound through [4 + 2] cycloadditions in **19** and through [2 + 2] cycloadditions in **20** and **21**, which are therefore expected to be less stable. A similar configuration is shown by **22**−**25** in which one or two of the six-membered rings are not bound, making these structures less symmetric. The most stable configuration, with an adsorption energy of −115.3 kcal mol^{-1}, is **19** with four pairs of [4 + 2] Si−C bonds (see Figure 1), while much lower adsorption energies of respectively −67.0 and −21.0 and −99.4, −74.0, −81.1, and −72.8 kcal mol^{-1} have been calculated for **20** and **21**, with two of the four Si−C bond pairs derived by [2 + 2] addition, and **22**−**25**, with only three or two pairs of Si−C bonds (see Table 2).

It is worth comparing the adsorption energies of the most stable of these pentacene adsorption configurations with the adsorption energy of benzene which, for the [4 + 2] addition on top of a silicon dimer, shows a value of −20.5 kcal mol^{-1} at the same level of theory.[29] The adsorption energies of **15** and **19** are higher than those of three and four isolated benzene molecules respectively by 18.9 and 33.3 kcal mol^{-1}. This is the result of two opposite effects: (i) a minor loss of aromatic stabilization energy for three or four rings of pentacene than for three or four isolated benzene rings; (ii) a higher strain energy due to the nonperfect matching of the fused rings with the underlying silicon dimers. The gain in pentacene adsorption energy clearly indicates that the first effect prevails. However, the strain energy contribution is important, as highlighted by a comparison of the adsorption energy of **19** with **7** (−115.3 vs −72.0 kcal mol^{-1}) or of **20** with **12** (−67.0 vs −48.4 kcal mol^{-1}), showing that **19** or **20** lose 28.7 or 29.8 kcal mol^{-1} with respect to two pentacene molecules adsorbed through two rings as in **7** or **12**.

Adsorption Perpendicular to Dimer Rows. Eight bonding configurations were considered for the adsorption of pentacene perpendicular to dimer rows (type B; see Chart 2). Structures **26**−**30** involve the adsorption of pentacene across two dimer rows, while structures **31**−**33** involve the adsorption across three dimer rows. The symmetric adsorption configurations across two dimers, **26**−**28**, are good candidates for subtype B-1 images, split into two parts, while the asymmetric configurations across two rows, **29** and **30** and the configurations across three dimers **31**−**33** are possible candidates for subtype B-2 images, split into three sections.

As shown in Table 2, the most stable configuration is **26**, see Figure 2, the only one bound with four pairs of Si−C bonds derived from [4 + 2] additions, with an adsorption energy of −128.3 kcal mol^{-1}, while **27**−**30** are all 30−110 kcal mol^{-1} higher in energy. The structures **31**−**33** across three rows, although bound through four Si−C pairs, are also quite high in

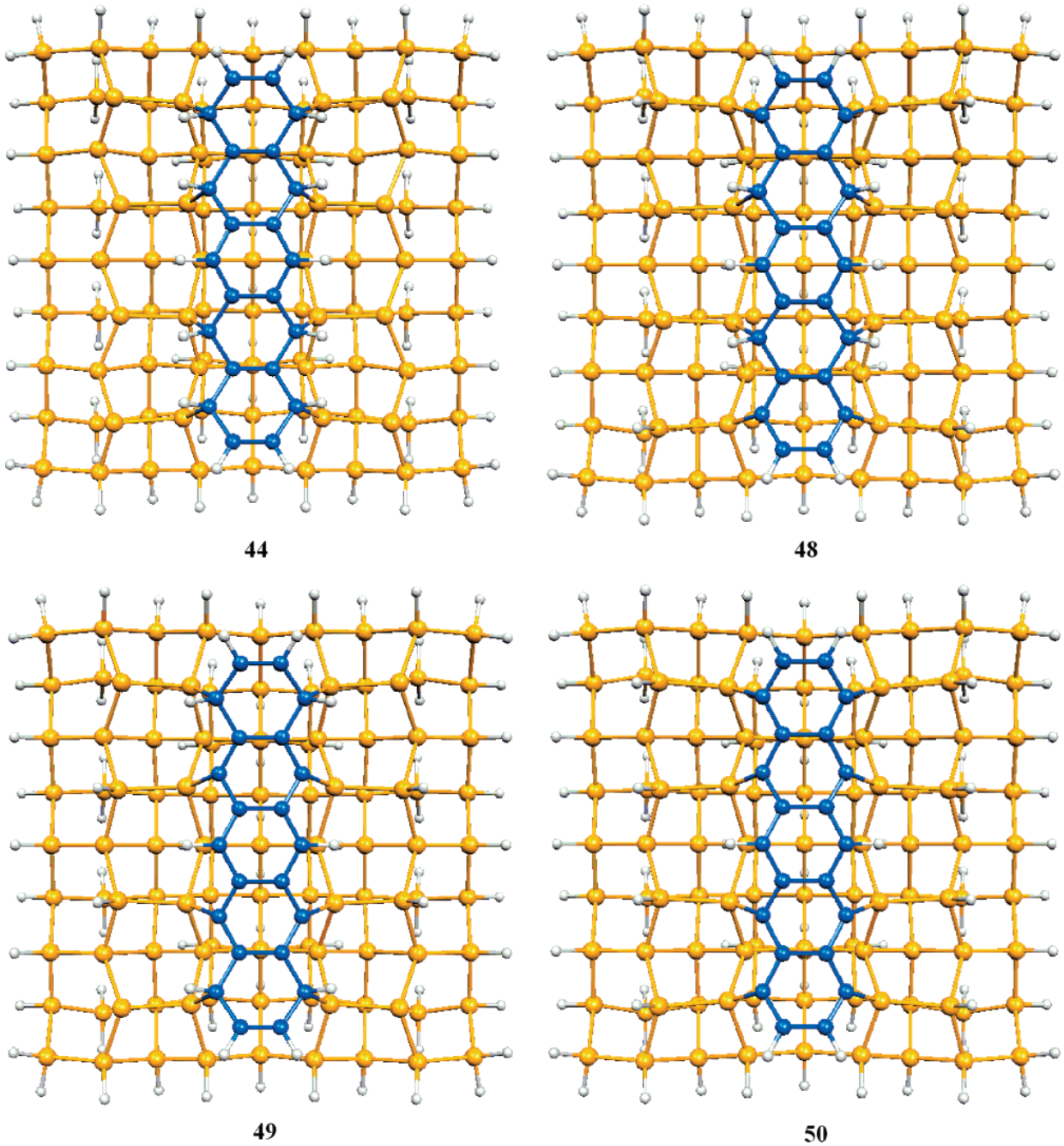

Figure 4. Optimized structures for the pentacene molecule adsorbed in between the dimer rows of the Si(100) surface **44** and the subsequent abstraction of two hydrogen atoms from the two outer **48** and the two adjacent inner rings **49** and of all the hydrogen atoms bound to sp^3 carbon atoms **50**.

energy, 40−120 kcal mol^{-1} above **26**, probably due to the high strain energy. A comparison of the adsorption energy of **26** with twice that of the analogous perpendicular configuration on two dimers of the same row, **13**, shows an energy loss of only 9.9 kcal mol^{-1}, much lower than that of 33.3 kcal mol^{-1} lost in the adsorption configuration of a dimer row **19**, thus indicating that the attachment of pentacene perpendicularly between two dimer rows involves a small strain energy. This is not surprising since the distance between the dimers rows (5.20 Å) fits pretty well with the distance between two nonadjacent rings of pentacene (4.92 Å).

Adsorption Diagonal to Dimer Rows. Among the several possible bonding configurations with pentacene diagonal across two dimer rows, type C, we considered 10 symmetric structures (with a C_2 axis) selected on the basis of (i) the highest number of Si−C bonds derived by [4 + 2]-like cycloadditions, (ii) the maximum matching of the formed Si−C bonds with the underlying surface topology, and (iii) the highest number of isolated aromatic rings and the highest conjugation of the remaining double bonds; see Chart 3. Structures **34** and **35** are attached through four pairs of Si−C bonds, **36**−**40** through three pairs, and **41**−**43** through only two pairs. Most structures leave the central ring aromatic, while in all the remaining rings the aromaticity is destroyed by the formation of the Si−C bonds, except for **43** which shows a central antracene unit. Due to the large size of these cluster models (106 Si, 22 C, and 82 H atoms including the pentacene molecule) and to the corresponding high computational load required to perform unrestricted DFT

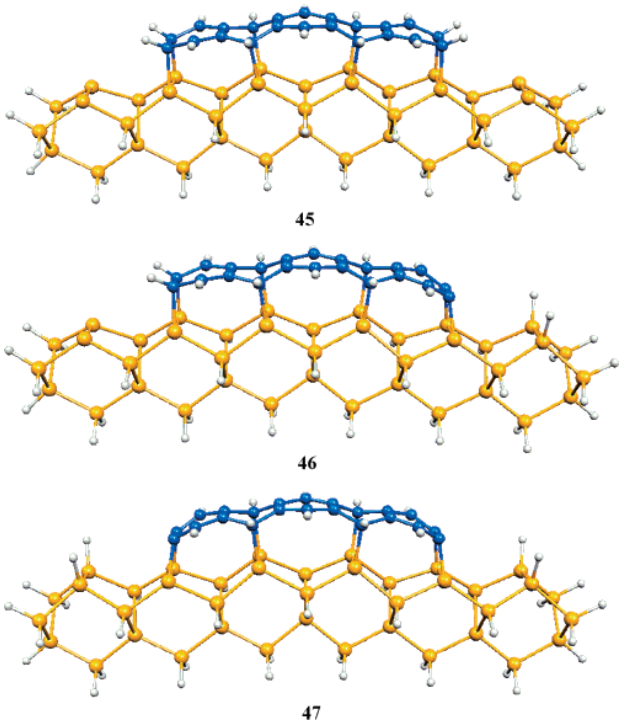

Figure 5. Optimized structures for the pentacene molecule adsorbed on top of the rows of the Si(100) surface **45** and the subsequent abstraction of two **46** and four **47** hydrogen atoms from the terminal sp^3 carbon atoms on the adjacent dimers.

calculations with a 6-31G(d,p) basis set on all the atoms, we performed a preliminary screening at semiempirical AM1 level[44] on all these 10 structures. This allowed us to select two structures, **40** and **43**, significantly lower in energy than the remaining ones, on which we carried out DFT geometry optimizations. The most stable configurations at DFT level is **40** (see Figure 3) with an adsorption energy of −79.7 kcal mol^{-1}, while **43**, bound through two pairs of Si−C bonds, is 43.8 kcal mol^{-1} less stable in energy (see Table 2). It is worth noting that these two structures present the highest number of aromatic ring, two in **40** and three in **43**. The diagonal configurations are therefore significantly less strongly bound than the most stable parallel or perpendicular configurations, probably due the high strain energy connected with the limited matching between the skew orientation of pentacene with respect to the dimer rows. These results are in agreement with experimental STM evidence, indicating very low or negligible population, depending on the experimental conditions, of the diagonal orientations.[19,21]

Adsorption "in between" Two Dimer Rows. We finally addressed "in between" adsorption configurations where pentacene is attached between two adjacent dimer rows lying parallel above the valley between them. We considered only the symmetric structure, **44** (see Chart 3 and Figure 4), where pentacene bridges four adjacent dimers of one row to the corresponding dimers of the second row in the $Si_{106}H_{68}$ cluster through four pairs of Si−C bonds.

On the basis of the relative energies calculated for the structures on the top of a dimer row, all the structures with less Si−C bonds or with bonds from a [2 + 2]-like cycloaddition are foreseen to be much higher in energy. Accordingly, a quite large adsorption energy of −117.8 kcal mol^{-1} was calculated for **44** (see Table 2), showing that this is one of the most stable configurations, in spite of the presence of dangling bonds on eight silicon atoms. This is in agreement with the results of a previous study of these authors on the adsorption configurations of benzene on Si(100), showing for the in between configuration across two dimer rows an adsorption energy close to that for the most stable [4 + 2] cycloaddition on top of a silicon dimer.[29]

Overall, our calculations indicate that the most stable adsorption configuration of pentacene on the Si(100) surface is the symmetric perpendicular structure **26** with an adsorption energy of −128.3 kcal mol^{-1}, with the symmetric parallel structure, **19**, 13.0 kcal mol^{-1} higher in energy. Structures **19** and **26** are therefore the best candidates for the A and B type STM images, respectively. Considering the issue of the subtypes, **19** and **26** would correspond to A-2 and B-1 subtypes, and the most plausible candidates for the A-1 subtype are **15** or **18**, while those for the B-2 subtype are **29** or **30**. The in between structure **44** is the second most stable configuration, only 10.5 kcal mol^{-1} higher than **26** and 2.5 kcal mol^{-1} lower than **19**, in agreement with its experimental detection with STM in a relatively high ratio. It is worth noting that the assignment of the various STM types or subtypes images to the considered adsorption configurations is actually an extremely difficult task. Indeed, the populations of the adsorption configurations are kinetically rather than thermodynamically determined and their evaluation would require a detailed knowledge of the mechanisms and the energy barriers of each single step involved in the formation of all the considered configurations. Even in the case that only thermodynamical factors are considered, the final population of an adsorption configuration may be determined by the stability of intermediate adsorption structures and not only by the stability of the final configuration. For instance, while **26** is 13.0 kcal mol^{-1} more stable than **19**, their formation requires first the bonding of pentacene on two dimers, leading to the key intermediates **13** and **7**, respectively, which differ only by 2.9 kcal mol^{-1}. Therefore, assuming that the formation of **7** and **13** is irreversible, **19** and **26** may form with similar populations, in spite of their very different adsorption energies.

C. C−H Bond Cleavage on the Adsorbed Pentacene: Products and Energetics. Since the bonding interaction between the pentacene molecules and the Si(100) surface has been revealed to be quite strong,[21,22] a question arises as to whether a dissociative adsorption occurs to some extent on the surface. Taking into account the experimental evidence of some Si−H vibrational modes at 2091 cm^{-1} on the FTIR spectrum of pentacene molecules on the Si(100) surface,[22] we addressed the issue of a C−H bond cleavage on the adsorbed pentacene molecules. To our knowledge, this is the first theoretical work analyzing both the energetics and the kinetics of the dissociative adsorption of pentacene on the Si(100) surface.

A previous study on the hypothetical C−H bond cleavage process of benzene on the Si(100) surface highlighted two adsorption configurations as good candidates for the hydrogen abstraction from the adsorbed benzene by surface silicon atoms and formation of Si−H bonds.[29] The first configuration is that obtained from the [2 + 2] addition of benzene on top of a single dimer and dissociates through hydrogen abstraction from the two Si-bound carbon atoms by the silicon atoms of the adjacent dimer on the same row. The second configuration is that obtained from the [4 + 2] addition across two rows and dissociates through the hydrogen abstraction from the two Si-bound carbon atoms by the dangling silicon atoms remaining on the dimers of the two rows. On the contrary, the most stable configuration, involving the [4 + 2] cycloaddition upon one dimer, showed a higher barrier for C−H bond cleavage. On the basis of these results, we evaluated only the thermodynamic

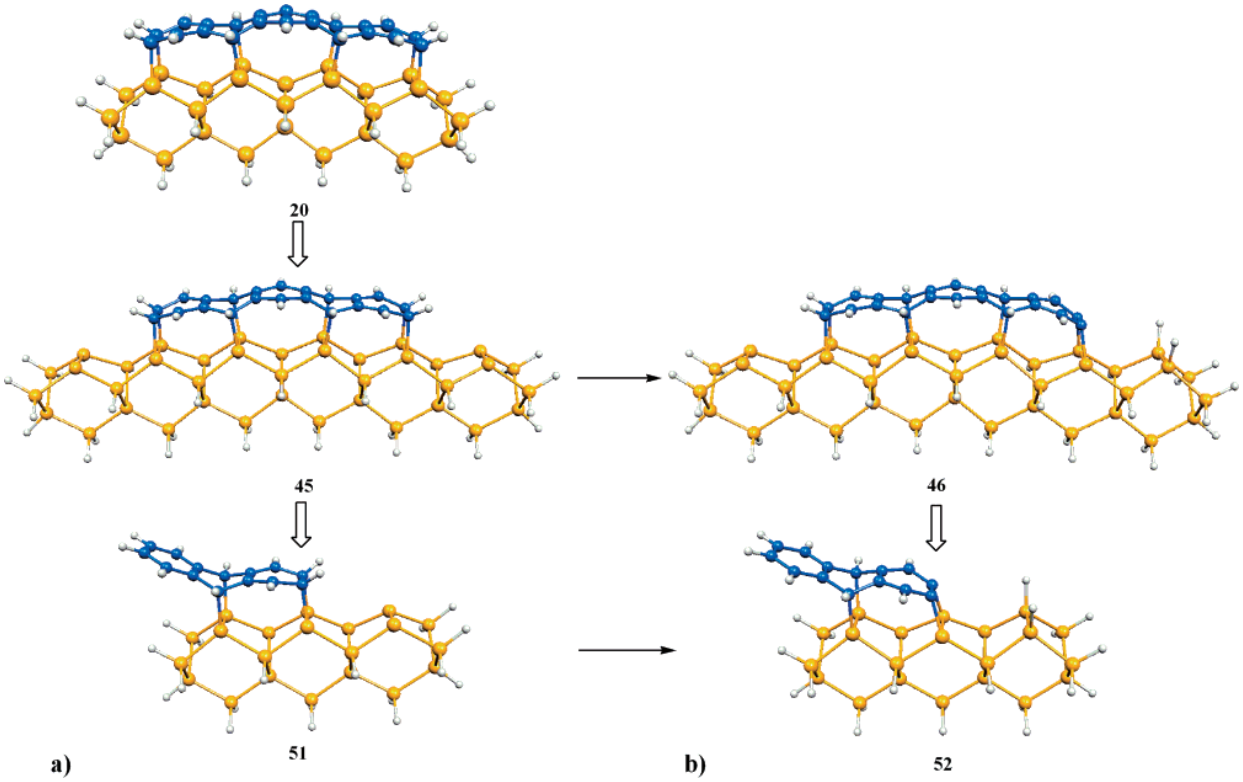

Figure 6. Correlation between extended and reduced models employed in the investigation of the kinetics of the C−H bond cleavage mechanism for the adsorbed pentacene: (a) adsorption on top of the dimer rows of the Si(100) surface; (b) the abstraction of two hydrogen atoms.

TABLE 3: Binding Energies (in kcal mol^{-1}) for the Stationary Points Reported in Schemes 3−5[a]

		Scheme 1		
51	**52**	**TS1**	**57**	**TS2**
-42.4 (−71.2)	−65.5 (−94.2)	−0.7 (−29.4)	−39.6 (−68.3)	−22.6 (−51.3)
		Scheme 2		
53	**55**	**TS3**	**58**	**TS4**
−8.3 (−117.8)	−48.6 (−158.1)	+22.0 (−87.5)	−32.4 (−141.9)	+35.3 (−78.0)
		Scheme 3		
54	**56**	**TS5**	**59**	**TS6**
−14.2 (−117.8)	−42.9 (−146.2)	+15.0 (−88.6)	−24.8 (−128.4)	+24.2 (−79.4)

[a] The values scaled with respect to binding energy value of structures **45** and **44** (see Figure 6 and 7, respectively) are reported in parentheses.

stabilities of those dissociation products obtained from the breaking of C−H bonds in the most stable of this kind of configurations, such as structures **20**, **23**, or **25** and **44**.

To analyze the C−H bonds breaking on the terminal sp^3 carbon atom of pentacene in the bonding configuration **20** and the subsequent transfer of the hydrogen atoms to the surface silicon atoms on an adjacent dimer of the same row, we considered a larger cluster model, constituted by six dimers on the same row. We first reoptimized the adsorption product of pentacene with two [4 + 2] and two [2 + 2] additions on the external rings (structure **45** in Figure 5), computing an adsorption energy of −71.1 kcal mol^{-1} (see Table 2), very close to the value of −67.0 kcal mol^{-1} calculated for **20**. We then considered the hydrogen abstraction from the terminal sp^3 carbon atoms on one side of pentacene to the surface silicon atoms on the adjacent dimer, leading to structure **46** (see Figure 5) with a binding energy of −92.8 kcal mol^{-1}. This dissociation process is exothermic by 21.7 kcal mol^{-1}, essentially due to the restoring of aromaticity on one external ring. We also considered the further hydrogen abstraction from the other side of pentacene, obtaining structure **47** (see Figure 5), that, with a binding energy of −114.3 kcal mol^{-1}, is 43.2 kcal mol^{-1} more stable than the adsorption configuration **45**. Indeed, the C−H bonds breaking process on the four terminal sp^3 carbon atoms leads to an adsorbed pentacene where three isolated benzene rings have restored the aromaticity, so that almost the entire aromatic stabilization energy of pentacene has been restored.

We then analyzed the hydrogen abstraction from the sp^3 carbon atoms of the in between configuration **44**. We first considered the abstraction of two hydrogen atoms from the two outer pentacene rings, leading to structure **48**, or from the two adjacent inner rings, leading to structure **49**, computing an adsorption energy of −160.8 and −141.6 kcal mol^{-1}, respectively (see Figure 4 and Table 2). The C−H dissociation of the outer rings of pentacene is thermodynamically more favored, as expected, since it leads to three isolated aromatic rings and

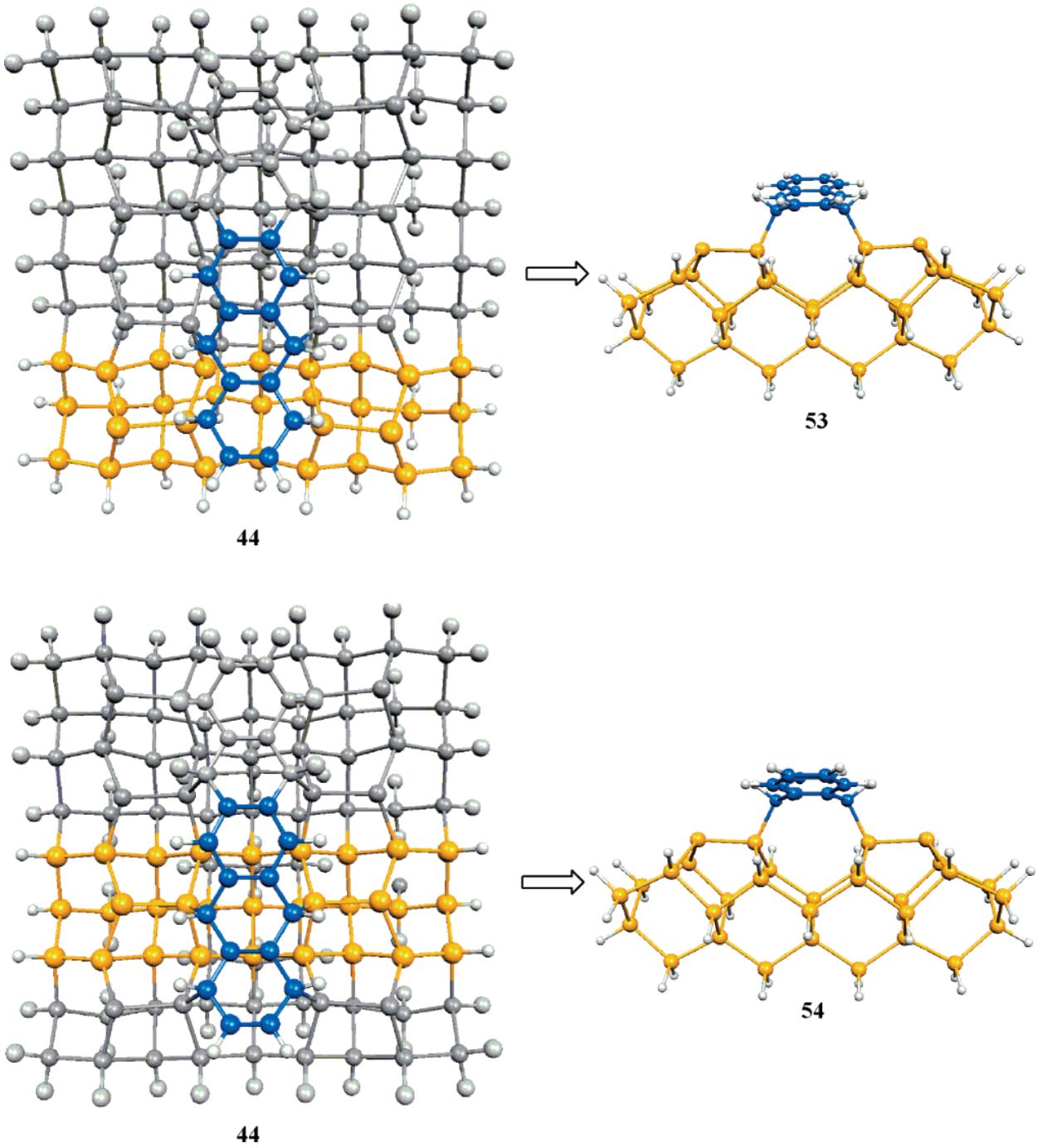

Figure 7. Correlation between the extended model **44**, where pentacene molecule is adsorbed in between dimer rows of the Si(100) surface, and the reduced models **53** and **54**, modeling respectively the adsorption on the outer and the inner ring of pentacene, employed for the investigation of the C−H bond cleavage mechanism. In structure **44** the atoms not employed in the reduced model are shown with gray color for clarity.

thus to a higher aromatic stabilization energy. We also verified the thermodynamic stability of the adsorbed pentacene upon the abstraction of all the hydrogen atoms bound to sp^3 carbon atoms, leading to structure **50** (see Figure 4), with a binding energy of −140.3 kcal mol^{-1}. Surprisingly, in spite of the higher number of aromatic rings, **50** is 20.5 kcal mol^{-1} less stable than **48**, probably due to the higher strain energy necessary to attain the planarity of the whole organic moiety. It is worth noting that the structures where several benzene rings have attained the aromaticity can represent a hybrid semiconducting organic−inorganic system and constitute an ideal platform for subsequent pentacene multilayer physisorption.

D. Kinetics of the C−H Bond Cleavage Mechanism on the Adsorbed Pentacene. We then analyzed the kinetics of the C−H bond cleavage process for the pentacene adsorption configurations **45** and **44**, leading to the thermodynamically more stable products **46** and **48** or **49**, respectively, looking for the transition states connecting the adsorption configurations to the final C−H broken structures. However, due to the size of the system, this is a computationally too demanding task, so we employed reduced models for the exploration of these potential energy surfaces. In particular, we replaced the adsorption configuration **45** with a reduced model, **51**, consisting of three dimers on the same row for the Si(100) surface and of an

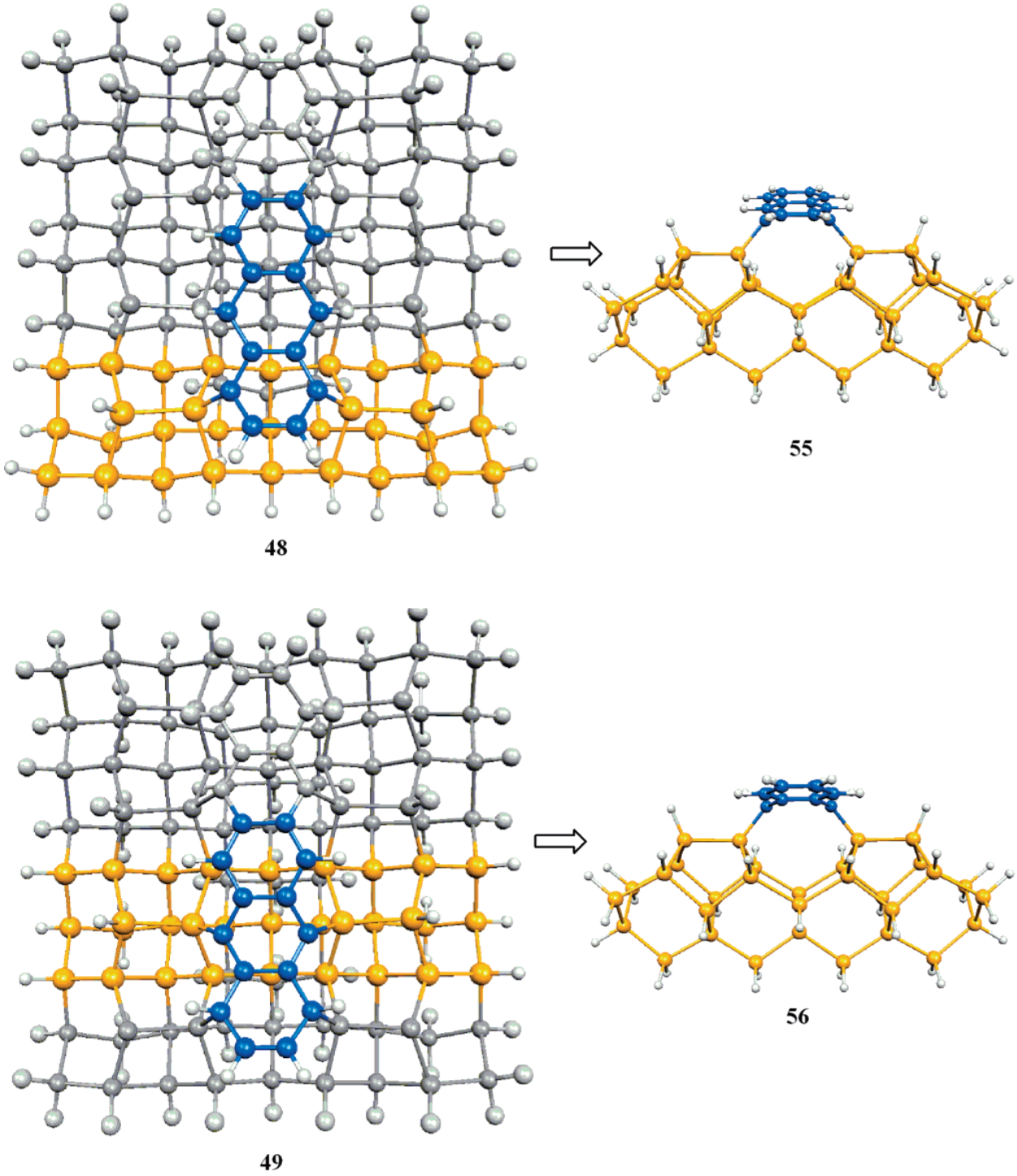

Figure 8. Correlation between the extended models **48** and **49**, where the C−H bond cleavage has occurred respectively on the outer and the inner rings of pentacene adsorbed in between silicon dimer rows, and the reduced models **55** and **56**, employed for the kinetic investigation. In structures **48** and **49** the atoms not employed in the reduced models are shown with gray color for clarity.

anthracene molecule (three fused benzene rings) for pentacene. We then optimized this reduced adsorption configuration **51** and the corresponding C−H cleaved product **52** (see Figure 6), finding stable structures with bonding energies of −42.4 and −65.5 kcal mol^{-1}, respectively (see Table 3). It is worth noting that although the adsorption energies of the reduced models **51** and **52** (−42.4 and −65.5 kcal mol^{-1}) are much lower than those of the complete models **45** and **46** (−71.1 and −92.8 kcal mol^{-1}) because of the lesser number of Si−C bonds, the dissociation process leading from **51** to **52** involves a gain in energy of 23.1 kcal mol^{-1}, a value very close to that of 21.7 kcal mol^{-1}, involved in the dissociation of the larger model **45** to **46**. This supports the use of the reduced model **51** to evaluate the kinetics of the C−H bond cleavage from the adsorption configurations **45**, provided that only relative energies of transition states, possible intermediates, and products with respect to **51** are considered and their absolute adsorption energies are scaled to that of the complete model **45**, i.e. to 71.1 kcal mol^{-1} (see Table 3 for a summary of the scaled binding energy values). Since **51** includes only half of **45** (i.e.,

SCHEME 3: Potential Energy Diagram for the C−H Bond Cleavage Mechanism from the Terminal sp^3 Carbon Atoms of the Anthracene Reduced Model Adsorbed on Top of the Rows of the Si(100) Surface through One [4 + 2] and One [2 + 2] Addition[a]

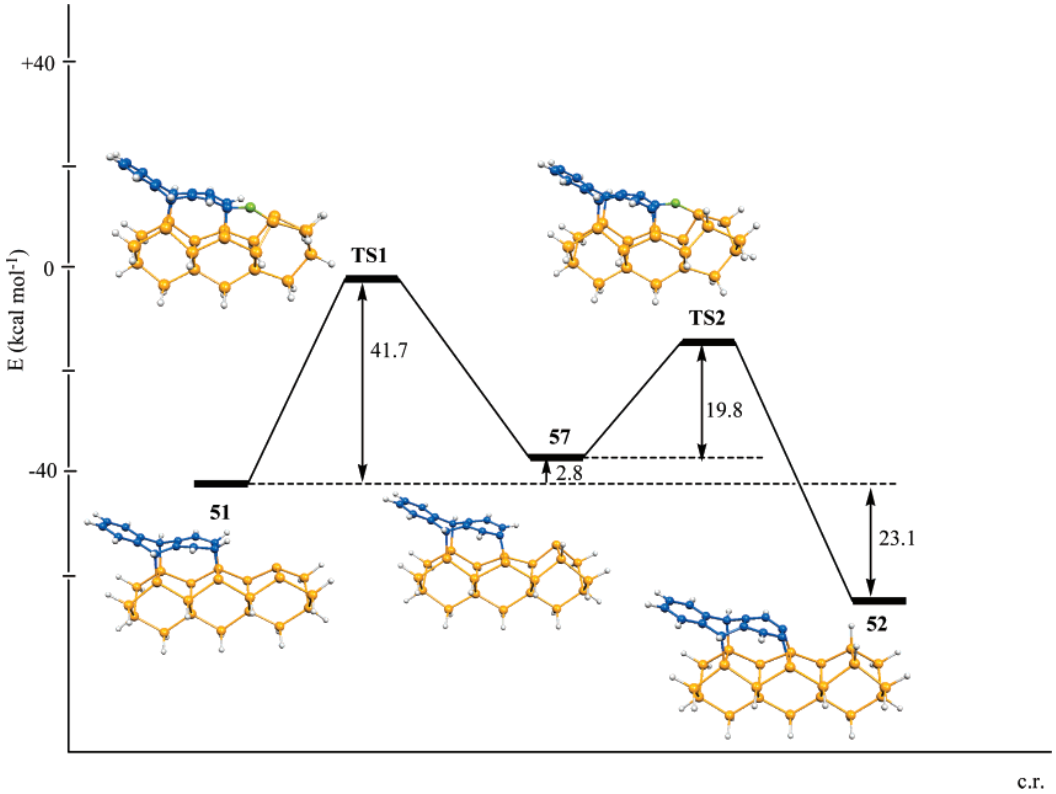

[a] The hydrogen atom involved in the C−H bond cleavage has a green color for clarity. The zero-energy scale refers to free anthracene and three dimer cluster reactants.

20), it can also be considered a good model for the C−H bond cleavage from the adsorption configurations **23** and **25**, scaling its adsorption energy to those of the latter configurations, i.e., to −74.0 and −72.8 kcal mol^{-1}.

Furthermore, we replaced the bonding configuration **44** with the reduced models, **53** and **54**, consisting of only two dimers on two adjacent rows for the Si(100) and an anthracene molecule for pentacene (see Figure 7). These two distinct models enabled us to consider separately the dissociation of the C−H bonds on the outer and the adjacent inner rings of pentacene, respectively. We then optimized the reduced adsorption configurations **53** and **54** and both C−H cleaved products **55** and **56** (the reduced models corresponding to **48** and **49**, respectively; see Figure 8) finding adsorption energies of −8.3 and −14.2 (for **53** and **54**) and −48.6 and −42.9 (for **55** and **56**) kcal mol^{-1}, respectively (see Table 3). Again, the adsorption energies of the reduced models **53** and **54** (−8.3 and −14.2 kcal mol^{-1}) are much lower than those for the in between configuration **44** (−117.8 kcal mol^{-1}) because of the lesser number of Si−C bonds, but they can still be employed to evaluate the kinetics of the C−H bond cleavage from the adsorption configuration **44**, considering only relative energies of transition states, intermediates, and products with respect to **53** or **54** and scaling their absolute adsorption energies to those of **44**, i.e. by 109.5 and 103.6 kcal mol^{-1}, respectively (see Table 3 for a summary of the scaled binding energy values).

We then investigated in detail the potential energy surface for each of the three considered C−H bond dissociation processes (**51** to **52**, **53** to **55**, and **54** to **56**, all consisting of the cleavage of two C−H bonds and the formation of two Si−H bonds), searching for all possible transition states and intermediates. The corresponding potential energy diagrams have been outlined in Schemes 3−5. For all processes we found a metastable intermediate corresponding to the cleavage of one of the two C−H bonds with formation of a Si−H bond and two transition states connecting it with the initial adsorption configuration and with the product where both C−H bonds are cleaved and Si−H bonds formed.

According to Scheme 3, two transition states, **TS1** and **TS2**, and one intermediate, **57**, have been identified on the potential energy surface leading from **51** to **52**. The first C−H bond breaking involves a high-energy barrier of 41.7 kcal mol^{-1} above **51** (0.7 kcal mol^{-1} below free reactants; see Table 3), while the breaking of the second C−H bond is energetically much easier, with an activation energy of 19.8 kcal mol^{-1} above **57** (22.6 kcal mol^{-1} below free reactants; see Table 3). The abstraction of the first hydrogen atom leads to the formation of a metastable biradical intermediate **57** (2.8 kcal mol^{-1} above **51**), characterized by the formation of only one Si−H bond, thus leaving one unpaired electron on the silicon dimer atom and on the external benzene ring, which then evolves easily through the abstraction of the second hydrogen atom to the final C−H cleaved products **52**, allowing the high-energy gain involved in the whole process. The optimized structure for **TS1** shows a lengthening of the C−H bond (1.554 Å), while a Si−H bond on the underlying silicon atom is forming (1.807 Å), with the silicon atom strongly buckled up to promote the abstraction of the hydrogen atom. Analogously, in **TS2** structure where the first Si−H bond has already formed, the carbon to silicon

SCHEME 4: Potential Energy Diagram for the C−H Bond Cleavage Mechanism from the Outer Rings of the Anthracene Reduced Model Adsorbed in between the Dimer Rows of the Si(100) Surface[a]

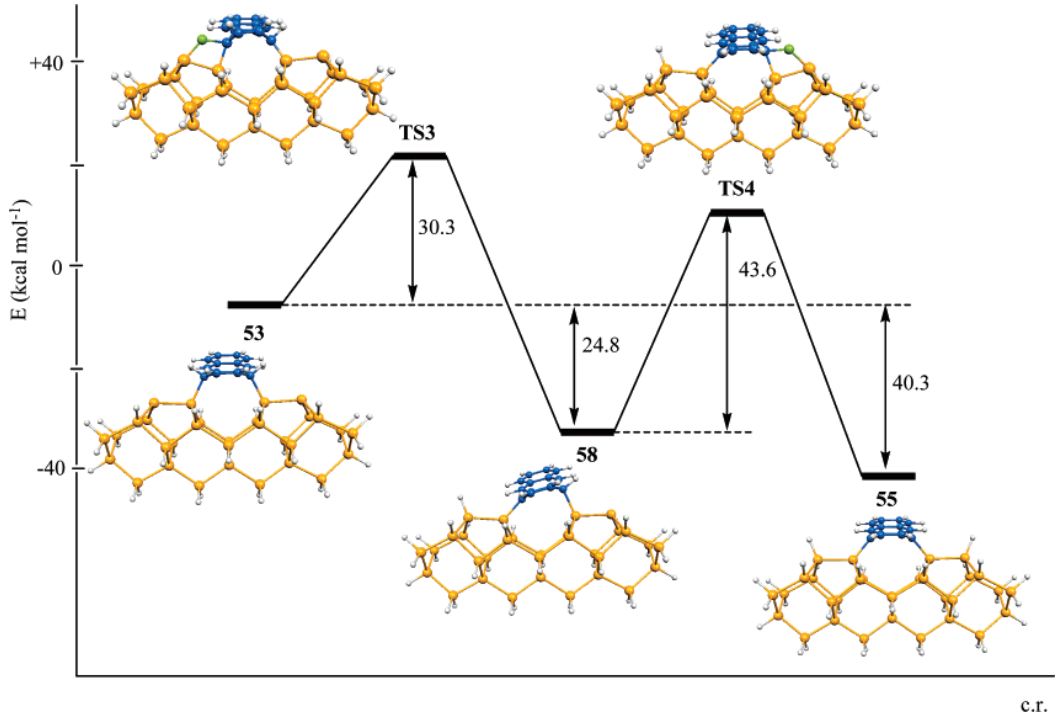

[a] The hydrogen atom involved in the C−H bond cleavage has a green color for clarity. The zero-energy scale refers to free anthracene and two dimer cluster reactants.

SCHEME 5: Potential Energy Diagram for the C−H Bond Cleavage Mechanism from the Adjacent Inner Rings of the Anthracene Reduced Model Adsorbed in between the Dimer Rows of the Si(100) Surface[a]

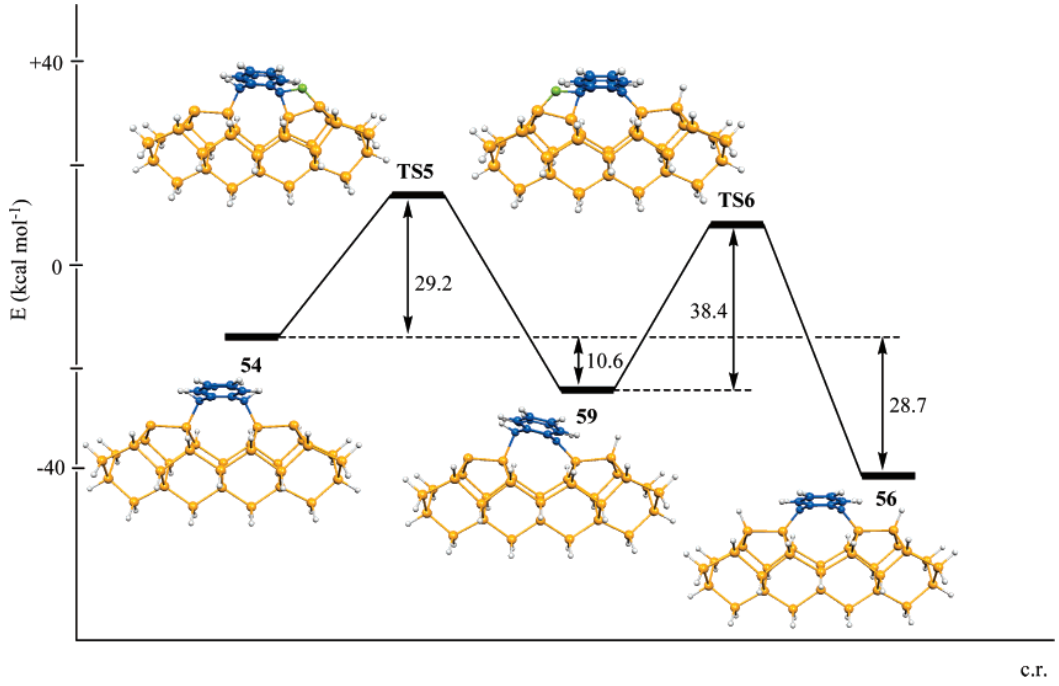

[a] The hydrogen atom involved in the C−H bond cleavage has a green color for clarity. The zero-energy scale refers to free anthracene and two dimer cluster reactants.

transfer of the second hydrogen atom is occurring: the C−H is lengthened (1.502 Å) and the Si−H bond is forming (1.873 Å).

As it is shown in Scheme 4, two transition states, **TS3** and **TS4**, and one intermediate, **58**, connecting them have been identified also on the reaction pathway leading from **53** to **55** involving the dissociation of the C−H bonds on the outer benzene ring of the acene molecule. The rate-determining step of this reaction pathway involves the C−H bond cleavage of the first hydrogen atom and passes through the transition state **TS3**, lying 30.3 kcal mol^{-1} above **53** (22.0 kcal mol^{-1} above

free reactants; see Table 3). The optimized geometry of **TS3** shows a distortion of both the benzene ring and the silicon dimer abstracting the hydrogen atom. The C−H bond is lengthened up to 1.648 Å, while the forming Si−H bond is still long, 1.828 Å, and the Si−C bond is shortened to 1.923 Å to promote the abstraction of the hydrogen. Once the Si−H bond has formed, **TS3** relaxes to the biradical intermediate **58**, where the benzene moiety is tilted toward the formed Si−H bond and one of the two unpaired electrons has shifted from one of the dangling silicon atom to the neighbor carbon atom. Due to the hydrogen abstraction, one of the two sp^3 carbon atoms of the ring has reached a sp^2 hybridization, giving rise to a radical benzene moiety with one unpaired electron conjugated with two double bonds, so that **58** is stabilized with respect to **53** by 24.8 kcal mol^{-1}, despite of the high distortion of the anthracene moiety. The abstraction of the second hydrogen atom passes through **TS4** and involves an energy barrier of 43.6 kcal mol^{-1} above **58** (35.3 kcal mol^{-1} above free reactants; see Table 3), leading to the final product **55**, where the aromaticity of benzene ring has been fully restored. The optimized structure of **TS4** shows the incipient abstraction of the second hydrogen atom, with a lengthened C−H bond of 1.613 Å and a forming Si−H bond of 1.868 Å.

The reaction pathway leading from **54** to **56** involving the cleavage of the C−H bonds on the inner benzene ring of the acene molecule shows a very similar potential energy diagram, see Scheme 5, with two transition states, **TS5** and **TS6**, and one intermediate, **59**, whose geometries are very close to those of **TS3**, **TS4**, and **58**, except for the involvement of a different six-member ring. However, slightly different energy barriers have been found, with the transition state **TS5** lying 29.2 kcal mol^{-1} above **54** (15.0 kcal mol^{-1} above free reactants; see Table 3). **TS5** then relaxes to the biradical intermediate **59,** which is stabilized with respect to **54** by 10.6 kcal mol^{-1}. The abstraction of the second hydrogen atom passes through **TS6** and involves a energy barrier of 38.4 kcal mol^{-1} above **59** (24.2 kcal mol^{-1} above free reactants; see Table 3), leading to the final product **56**, where the aromaticity of benzene ring has been fully restored.

The results of our kinetic analysis on the reduced models shown in Figures 6−8 suggest for the C−H bond cleavage on the adsorbed pentacene in the in between configurations **44** a highest energy barrier of 29−30 kcal mol^{-1} (i.e., 88−89 kcal mol^{-1} below free reactants; see Table 3), much lower than the desorption energy of 117.8 kcal mol^{-1}, thus indicating that this is a feasible process at room temperature in agreement with experimental evidence. On the other hand, C−H bond cleavage from adsorption configurations characterized by a [2 + 2] cycloaddition of one outer ring of pentacene, such as **20**, **23**, or **25**, shows a highest energy barrier of 41.7 kcal mol^{-1} (i.e., 29.4 kcal mol^{-1} below free reactants; see Table 3), again lower than the desorption energies of ca. 70 kcal mol^{-1}, suggesting that this is a feasible process only at temperatures above ca. 400 K.

Conclusions

In this paper, we have performed an extensive DFT investigation on the main adsorption configurations of pentacene on the Si(100) surface and on the possible pathways for the following C−H bond cleavage. To our knowledge, this is the first theoretical work analyzing both the energetics and the kinetics of the dissociative adsorption of pentacene on the Si(100) surface.

Several possible configurations for the adsorption of pentacene on the Si(100) surface, suggested in previous experimental and theoretical studies, were examined. We considered possible candidates for all the orientations of pentacene experimentally observed with STM, i.e., type A (on the top of silicon dimer rows), type B (perpendicular to the dimer rows), type C (diagonal to the dimer rows), and in between (between two adjacent dimer rows). On overall, our calculations indicate that the most stable adsorption configuration of pentacene on the Si(100) surface is the symmetric perpendicular structure with an adsorption energy of −128.3 kcal mol^{-1}, with the symmetric parallel structure 13.0 kcal mol^{-1} higher in energy. These structures are therefore the best candidates for the A and B type STM images, respectively. The in between structure is the second most stable configuration, only 10.5 kcal mol^{-1} higher than the perpendicular structure, in agreement with its experimental detection with STM.

More importantly, we then analyzed the kinetics of the C−H bond cleavage process from two kinds of adsorbed configurations of pentacene from which the breaking of two C−H bonds can be accessible: one on top of a silicon dimer row with one or both outer benzene rings di-σ−bonded through a [2 + 2] cycloaddition; one with one or more pentacene rings 1,4 di-σ−bonded across two dimer rows. We investigated in detail the potential energy surface for the C−H bond dissociation from these configurations (all consisting of the cleavage of C−H and the formation of Si−H bonds) searching for all possible transition states and intermediates. The kinetically most favorable reactive channel is that from the in between configuration and involves the separate abstraction of two hydrogen atoms on the sp^3 carbon atoms by the two silicon atoms of the two dimers bearing unpaired electrons, with a highest energy barrier of 29−30 kcal mol^{-1}. Notably, this energy barrier is much lower than the desorption energy of pentacene from the same configuration, 117.8 kcal mol^{-1}, and is therefore expected to be accessible at room temperature, in agreement with experimental evidence.

It is worth comparing these results for the kinetics of the C−H bond dissociation of pentacene adsorbed on Si(100) with those recently reported by us for the kinetics of the C−H bond dissociation of benzene adsorbed on the same surface.[29] For benzene, a reaction path starting from the in between configuration was found analogous to that calculated for pentacene, with a metastable intermediate corresponding to the cleavage of one of the two C−H bonds and two transition states connecting it with the initial adsorption configuration and leading to the product where both C−H bonds are cleaved. Although the slightly different computational approach makes a quantitative comparison questionable, the energy barrier calculated for the cleavage of the first C−H bond for benzene was found significantly higher than that for pentacene, ca. 50 vs 30 kcal mol^{-1}. More importantly, the energy barrier for the cleavage of the C−H bond from the in between configuration of benzene was found much higher than the desorption energy of benzene from the same configuration, 20.3 kcal mol^{-1}, and therefore this process is not expected to be accessible at temperature below benzene desorption, in agreement with the absence of any experimental evidence of C−H bond cleavage for this monocyclic aromatic hydrocarbon.

Acknowledgment. This work was supported by the MIUR (Programma di Ricerca FIRB, year 2003, Research Title "Molecular compounds and hybrid nanostructured materials with resonant and non-resonant optical properties for photonic devices", and PRIN 2006, Contract No. 20006038520_001) and by the CNR.

Supporting Information Available: Optimized geometries and total electronic energies for all the stationary points described in this work. This material is available free of charge via the Internet at the http://pubs.acs.org.

References and Notes

(1) Hamers, R. J. *Nature* **2001**, *412*, 489.
(2) Dimitrakopoulos, C. D.; Malenfant, P. R. L. *Adv. Mater.* **2002**, *14*, 99.
(3) Katz, H. E.; Bao, Z. *J. Phys. Chem. B* **2000**, *104*, 671.
(4) Dimitrakopoulos, C. D.; Mascaro, D. J. *IBM J. Res. Dev.* **2001**, *45*, 11.
(5) Rogers, J. A.; Bao, Z. *J. Polym. Sci., Part A* **2002**, *40*, 3327.
(6) Hamers, R. J.; Hovis, J. S.; Greenlief, C. M.; Padowitz, D. F. *Jpn. J. Appl. Phys.* **1999**, *38*, 3879.
(7) Yates, J. T., Jr. *Science* **1998**, *279*, 335.
(8) Waltenburg, H. N.; Yates, J. T. *Chem. Rev*. **1995**, *95*, 1589.
(9) Hamers, R. J.; Wang, Y. *Chem. Rev*. **1996**, *96*, 1261.
(10) Buriak, J. M. *Chem. Rev.* **2002**, *102*, 1271. Bent, S. F. *Surf. Sci.* **2002**, *500*, 351.
(11) Minakata, T.; Nagoya, I.; Ozaki, M. *J. Appl. Phys.* **1991**, *69*, 7354.
(12) Laquindanum, J. G.; Katz, H. E.; Lovinger, A. J.; Dodabalapur, A. *Chem. Mater.* **1996**, *8*, 2542.
(13) Ruiz, R.; Nickel, B.; Koch, N.; Feldman, L. C.; Haglund, R. F.; Kahn, A.; Scoles, G. *Phys. Rev. B* **2003**, *67*, 125406.
(14) Lin, Y.-Y.; Gundlach, D. J.; Nelson, S. F.; Jackson, T. N. *IEEE Electron Device Lett.* **1997**, *18*, 606.
(15) Kelley, T. W.; Boardman, L. D.; Dunbar, T. D.; Muyres, D. V.; Pellerite, M. J.; Smith, T. Y. P. *J. Phys. Chem. B* **2003**, *107*, 5877.
(16) Heringdorf, F.-M. Z.; Reuter, M. C.; Tromp, R. M. *Nature* **2001**, *412*, 517.
(17) Ozaki, H. *J. Chem. Phys.* **2000**, *113*, 6361.
(18) Kymissis, I.; Dimitrakopoulos, C. D.; Purushothaman, S. *IEEE Trans. Electron Devices* **2001**, *48*, 1060.
(19) Kasaya, M.; Tabata, H.; Kawai, T. *Surf. Sci.* **1998**, *400*, 367.
(20) Suzuki, T.; Sorescu, D. C.; Yates, J. T., Jr. *Surf. Sci.* **2006**, *600*, 5092.
(21) Hughes, G.; Roche, J.; Carty, D.; Cafolla, T.; Smith, K. E. *J. Vac. Sci. Technol., B* **2002**, *20*, 1620.
(22) Weidkamp, K. P.; Hacker, C. A.; Schwartz, M. P.; Cao, X.; Tromp, R. M.; Hamers, R. J. *J. Phys. Chem. B* **2003**, *107*, 11142.
(23) Yamaguchi, T. *J. Phys. Soc. Jpn.* **1999**, *68*, 1321.
(24) Choudharya, D.; Clancy, P.; Bowler, R. *Surf. Sci.* **2005**, *578*, 20.
(25) Tsetseris, L.; Pantelides, S. T. *Appl. Phys. Lett.* **2005**, *87*, 233109.
(26) Taguchi, Y.; Fujisawa, M.; Takaoka, T.; Okada, T.; Nishijima, M. *J. Chem. Phys*. **1991**, *95*, 6870.
(27) Lopinski, G. P.; Fortier, T. M.; Moffat, D. J.; Wolkow, R. A. *J. Vac. Sci. Technol., A* **1998**, *16*, 1037.
(28) Wolkow, R. A.; Lopinski, G. P.; Moffatt, D. J. *Surf. Sci.* **1998**, *416*, L1107.
(29) Nunzi, F.; Sgamellotti, A.; Re, N. *J. Phys. Chem. C* **2007**, *111*, 1392.
(30) Widjaja, Y.; Musgrave, C. B. *Surf. Sci.* **2000**, *469*, 9.
(31) *Jaguar*, v. 6.0; Schrodinger, Inc.: New York, 2005.
(32) Becke, A. D. *J. Chem. Phys.* **1993**, *98*, 1372.
(33) Becke, A. D. *J. Chem. Phys*. **1993**, *98*, 5648.
(34) Lee, C.; Yang, W.; Parr, R. G. *Phys. Rev. B* **1988**, *37*, 785.
(35) Mui, C.; Bent, S. F.; Musgrave, C. B. *J. Phys. Chem. A* **2000**, *104*, 2457.
(36) Barriocanal, J. A.; Doren, D. J. *J. Phys. Chem. B* **2000**, *104*, 12269.
(37) Widjaja, Y.; Mysinger, M. M.; Musgrave, C. B. *J. Phys. Chem. B* **2000**, *104*, 2527.
(38) Nunzi, F.; Sgamellotti, A.; Re, N. *J. Phys. Chem. B* **2004**, *108*, 10881.
(39) Nunzi, F.; Sgamellotti, A.; Re, N. *J. Phys. Chem. B* **2006**, *110*, *7682*.
(40) Guner, V.; Khuong, K. S.; Leach, A. G.; Lee, P. S.; Bartberger, M. D.; Houk, K. N. *J. Phys. Chem. A* **2003**, *107*, 11445.
(41) Kang, J. K.; Musgrave, C. B. *J. Chem. Phys.* **2001**, *115*, 11040. Zhao, Y.; Truhlar, D. G. *J. Phys. Chem. A* **2004**, *108*, 6908. Zhao, Y.; Truhlar, D. G. *J. Phys. Chem. A* **2005**, *109*, 5656. Zhao, Y.; Schultz, N. E.; Truhlar, D. G. *J. Chem. Theory Comput.* **2006**, *2*, 364.
(42) Jung, Y. M. S. Gordon *J. Am. Chem. Soc*. **2005**, *127*, 3131.
(43) Wannere, C. S.; Sattelmeyer, K. W. H. F.; Schaefer, P. R., III; Schleyer, P. v. R. *Angew. Chem., Int. Ed.* **2004**, *43*, 4200 and references therein.
(44) Dewar, M. J. S.; Zoebisch, E. G.; Healy, E. F. J. J. P. Stewart *J. Am. Chem. Soc*. **1985**, *107*, 3902.